SLAC-PUB-14341

Hidden magnetic configuration in epitaxial $La_{1-x}Sr_xMnO_3$ films

J.-S. Lee,[1] D. A. Arena,[1] P. Yu,[2] C. S. Nelson,[1] R. Fan,[3] C. J. Kinane,[3] S. Langridge,[3] M. D. Rossell,[4] R. Ramesh,[2,5] and C.-C. Kao[6]

[1]*National Synchrotron Light Source, Brookhaven National Laboratory, Upton, New York 11973, USA*
[2]*Department of Physics, University of California, Berkeley, CA 94720, USA*
[3]*ISIS, Harwell Science and Innovation Campus, STFC, Oxon OX11 0QH, UK*
[4]*National Center for Electron Microscopy, Lawrence Berkeley National Laboratory, Berkeley, CA 94720, USA*
[5]*Materials Science Division, Lawrence Berkeley National Laboratory, Berkeley, CA 94720, USA*
[6]*Stanford Synchrotron Radiation Light source, SLAC National Accelerator Laboratory, Menlo Park, CA 94025, USA*

We present an unreported magnetic configuration in epitaxial $La_{1-x}Sr_xMnO_3$ (x∼0.3) (LSMO) films grown on strontium titanate (STO). X-ray magnetic circular dichroism indicates that the remanent magnetic state of thick LSMO films is opposite to the direction of applied magnetic field. Spectroscopic and scattering measurements reveal that the average Mn valence varies from mixed Mn^{3+}/Mn^{4+} to an enriched Mn^{3+} region near the STO interface, resulting in a compressive lattice along a, b-axis and a possible electronic reconstruction in the Mn e_g orbital ($d_{3z^2-r^2}$). This reconstruction may provide a mechanism for coupling the Mn^{3+} moments antiferromagnetically along the surface normal direction, and in turn may lead to the observed reversed magnetic configuration.

PACS numbers: 75.30.-m, 75.47.Lx, 75.70.Cn, 75.30.Kz

The development of sophisticated thin-film deposition techniques, such as pulsed laser deposition and oxide molecular beam epitaxy [1, 2], which can produce abrupt interfaces with nearly atomic-level precision, has led to the widespread incorporation of correlated electron materials in device structures. New devices exploiting atomic-level control, such as all-oxide spin FETs [3], magnetic tunnel junctions (MTJs) [4] and multiferroic memory [5], often include mixed-valence manganites as metallic contacts with well-defined magnetic ordering. Mixed valence manganites, in which a delicate interaction between electronic, orbital, magnetic and structural degrees of freedom produces rich phase diagrams reflecting the competing, nearly-degenerate ground states, have been under intense investigation for decades [6, 7]. In this class of materials, $La_{1-x}Sr_xMnO_3$ is an attractive material for incorporation into spin-dependent electronic devices [8, 9]. However, the balance of stoichiometry and strain can affect the properties of $La_{1-x}Sr_xMnO_3$ films in unexpected ways [10], as seen in the rich phase diagram that develops at low hole doping (x∼1/8) [11]. At higher Sr doping the phase diagram simplifies considerably and $La_{1-x}Sr_xMnO_3$ with x∼0.3, hereafter referred to as simply LSMO, is a wide-bandwidth ferromagnetic metal with a high Fermi-level spin polarization [12]. These characteristics make LSMO a popular choice for electrodes in devices utilizing correlated electron materials.

In heterogenous, layered devices, the details of the magnetic state at interfaces greatly affect the electron and spin transport [13]. While recent advances in thin-film deposition techniques can produce atomically abrupt interfaces, the magnetic order need not follow the sharp transitions in the chemical order across the interface. For example, in LSMO/non-magnet interfaces, a reduction of the ferromagnetic (FM) moment in the LSMO near the interface often occurs [14, 15]. Such effects are thought to reduce the tunneling magneto-resistance in MTJs [4]. In this letter, we show that the magnetic structure of simple, monolithic LSMO films can be more complicated than previously reported. Specifically, the interaction between the FM LSMO layer and the $SrTiO_3$ (STO) substrate leads to a profile of Mn valence and orbital anisotropy that results in an unexpected magnetic configuration. Instead of simply reducing the FM aligned moments in the vicinity of an interface, our x-ray magnetic circular dichroism (XMCD) data indicate that a *reversal* of the FM moments sampled by XMCD in total electron yield occurs at remanence. The remanent reversal of the LSMO moments is a strong function of the total LSMO thickness, applied magnetic field, and temperature. Also, by combining the x-ray spectroscopy with x-ray scattering, we reveal the presence of a region near the interface with the STO with an enriched Mn^{3+} concentration. X-ray diffraction data indicate that the presence of a near-substrate region with enriched Mn^{3+}, which has anisotropic $d_{3z^2-r^2}$ orbital character, undergoes a structural fluctuation at a temperature commensurate with the onset of the reversed magnetic moments at remanence. Our results have important implications in the use of LSMO and similar oxide materials in engineered structures, as well as suggesting an additional and controllable degree of freedom in exploiting correlated electron materials.

Epitaxial LSMO films were grown on (001) Nb-doped STO substrates (TiO_2 terminated surface) using pulsed laser deposition. The detailed growth conditions were described in a previous publication [16]. To understand, in microscopic detail, the development of the magnetic profile in LSMO films grown on STO(001), we under-

Work supported in part by US Department of Energy contract DE-AC02-76SF00515.

took XMCD measurements at the Mn $L_{2,3}$-edges using total electron yield (TEY), which is sensitive to the near-surface region (probing depth: ∼40-100 Å), for a set of films with different LSMO thickness. We obtained the dichroic spectra below the Curie temperature (T_c) by reversing the polarity (right or left circular) of the incident photon beam and by changing the direction of the magnetic field at fixed polarity. The spectra (ρ^+ and ρ^-), which result from Mn $2p \rightarrow 3d$ dipole transitions, represent the parallel and antiparallel alignment of the magnetization direction with the photon helicity vector, respectively. The geometry was measured at a 30° beam incidence and the degree of circular polarization was 70%. During the XMCD measurements, we employed two kinds of energy scans (see Fig. 1(a)): *h-XMCD* measured at the saturated magnetic-state using a holding H-field, and *p-XMCD* measured at the remanent magnetic-state using a pulsed H-field greater than the saturating field for these samples. The XMCD experiments were carried out at beamline U4B at the National Synchrotron Light Source (NSLS).

In a 90 unit cell (1 UC∼3.9 Å) sample, where the LSMO is expected to behave in a bulk-like fashion, we observed an unusual behavior: a reversal of the dichroic signals between the h-XMCD and p-XMCD measurements (Fig. 1(b) top). This implies that the remanent state of the LSMO differs from the saturated one; the near-surface spin configuration in the remanent state is antiparallel to the saturated state. To eliminate possible artifacts in the measurement and hence confirm whether this effect is intrinsic to the sample, we also measured the XMCD spectra by changing the photon helicity rather than the reversing the applied field. The results were identical. Furthermore, polarized neutron reflectivity measurements, which can probe the entire sample thickness, confirm this reversal [17]. Figure 1(b), bottom, shows the behavior of the reversed dichroic signal by examining a series of films of differing LSMO thickness (4-90 UC). Turning first to the h-XMCD spectra, we observe only a change in the intensity of the XMCD with a reduction in film thickness, reflecting the reduction of the T_c of the film and the corresponding reduction in the magnetization [18]. On the other hand, the trend in the p-XMCD suddenly shows a change in spectral sign between 11 and 9 UC. Evidently, the reversal of the p-XMCD is triggered at a specific thickness. Below this thickness, the h-XMCD and p-XMCD retain the same orientation; above this thickness, the near-surface region adopts an anti-parallel orientation relative to the H-field.

The p-XMCD data as a function of film thickness suggest that there may be an intermediate LSMO layer along the surface normal. To further examine the composition of this layer, we examined the x-ray absorption spectroscopy (XAS) at the Mn $L_{2,3}$-edges to investigate the mixed-valence state of the Mn in the films. For the 90 UC sample, the results agree with previously published results on $La_{1-x}Sr_xMnO_3$ [19, 20] and we thus confirm the x∼0.3 stoichiometry of the sample. In the case of the 90 and 55 UC samples, the shapes of the spectra appear similar. Considering the probing depth of the TEY signal, the measurements correspond in both cases to the near-surface region with negligible contributions from the

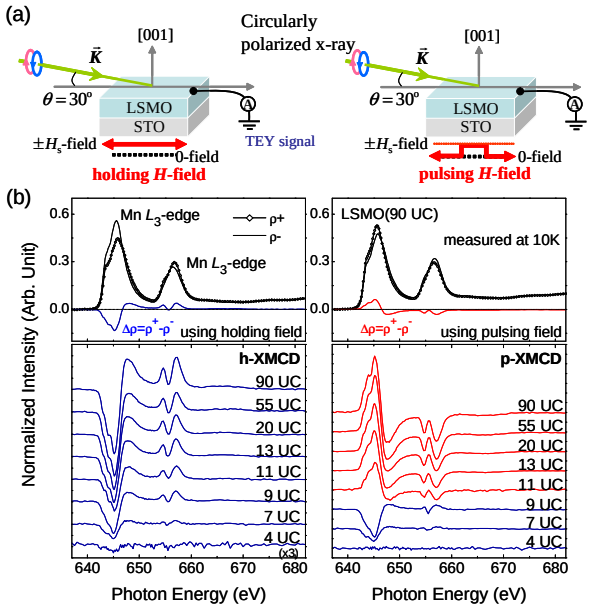

FIG. 1: (Color online) (a) Schematic picture of experimental configurations for h-XMCD (left) and p-XMCD (right). (b) Thickness dependent XMCD results on LSMO at T=10K. Left is h-XMCD. Right is p-XMCD.

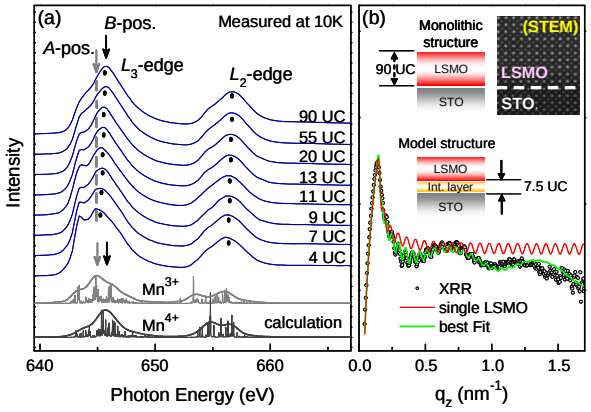

FIG. 2: (Color online) (a) Thickness dependent XAS on LSMO. The A and B-positions are identified by Mn^{3+} and Mn^{4+} via the model calculation, respectively. (b) XRR data and model calculations for LSMO(90UC)/STO. The schematic diagrams represent the monolithic structure (single layer) and best-fit structure (double layer). Scanning transmission electron microscopy (STEM) demonstrates the high quality of the sample.

LSMO layers near the STO interface. On the other hand, we observed a significant change in the spectra on the thinner samples. In the Mn $L_{2,3}$ XAS spectrum for the 90 UC sample, we distinguished two energy states, 644.8 eV (A-position), and 645.7 eV (B-position). To support the assignment of the peaks, we simulated the Mn^{3+} and Mn^{4+} spectra using the configuration interaction model (Fig. 2(a), bottom) [21, 22]. The A- and B-positions are related to spectral features originating primarily from Mn^{3+} and Mn^{4+} valence states, respectively. For thinner samples, the A-position feature became relatively enhanced in the spectrum (see the shifted B-position: dots in Fig. 2(a)), although the mixed valence state remained. The spectra imply that the stoichiometry of the LSMO films in not uniform along the surface normal of the film, which is consistent with the recent electron energy-loss spectroscopy results [23, 24].

The variation of the sample stoichiometry along the surface normal direction should lead to a change in the charge density. To examine this, we undertook x-ray reflectivity (XRR) measurements with E=7.62 keV at beamline X16B at NSLS (Fig. 2(b)). Small oscillations (Kiessig fringes) in XRR reflect the total thickness, while longer oscillations originate from the intermediate layer, or in combinations between the two spatial frequencies. Our XRR data clearly reveal the interference effect of the Kiessig fringes on the LSMO(90 UC)/STO film, which effectively rules out a single layer structural model for the LSMO (red curve, estimated total thickness 90 UC). We adopted a two-layer model, consisting of a mixed valence layer (Mn^{3+}:Mn^{4+}= 0.7:0.3) and an intermediate layer (relatively enriched in Mn^{3+}), and fitted the XRR data using a Parratt formalism [25]. A best fit model to the XRR (green curve) reproduces the Kiessig fringes on the 90 UC sample with the intermediate layer (fitted thickness 7.5 UC), and the mixed valence layer (fitted thickness 82.5 UC). We note that other samples exhibited similar results with two-layer structure and same intermediate thickness. Combining the XAS and XRR data, we confirm an inhomogeneous distribution of the Mn valence: an intermediate layer of an Mn3+ enriched state adjacent to the STO interface and an over layer with a stoichiometry closer to the expected LSMO.

To more fully explore the role of the intermediate layer, we measured the temperature-dependence of the Mn XMCD on a LSMO(90 UC)/STO film. Figure 3(a) shows the p-XMCD spectrum with different temperatures. As depicted in Fig. 1(b), the p-XMCD at the Mn L_3 edge (645 eV) is positive (indicating an opposite behavior to the h-XMCD) at low temperature. However, the sign of p-XMCD clearly reverses above and below T=125K; above this temperature, the h-XMCD and p-XMCD are in alignment. We note that other samples exhibited anomalous magnetic behavior around 125K. This anomalous temperature, $T_a = 125K$, is completely different with T_c on LSMO(90 UC) measured by SQUID

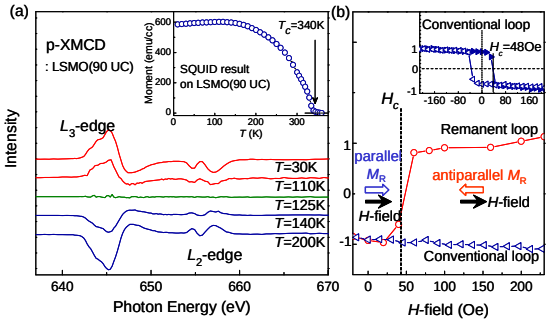

FIG. 3: (Color online) (a) Temperature dependent XMCD of LSMO(90 UC)/STO. Inset shows SQUID data on 90 UC. (b) Hysteresis loop (M vs. H curves) using two different applied field modes: conventional and remanent loop. Inset shows the entire conventional loop.

magnetometry (Fig. 3(a) inset). Considering the estimated thickness (7.5 UC) of the intermediate layer, the magnetism of the Mn^{3+} enriched state appears to develop below T_a. From these data, a picture emerges where the development of a remanent moment for the intermediate layer differs from that of the general mixed-valence layer of the LSMO. Below 125K, after the development of the magnetic moment in the near-substrate, enriched Mn^{3+} region, the coupling of the remanent magnetization (M_R) of the region sampled by XMCD becomes antiparallel to the applied H-field, resulting in the reversed p-XMCD behavior.

Furthermore, we explored this anomalous M_R behavior using field dependence, Fig. 3(b): hysteresis loop (M vs. H curve). Similar to our p-XMCD and h-XMCD methods, we measured both conventional (Fig. 3(b) inset), field swept hysteresis, where measurement of the TEY intensity is monitored as the applied field is swept smoothly from a negative saturating field to a positive saturating field and back again, and also remanent hysteresis loop, where the field is pulsed to a specific value and intensity is measured at remanence. In the high H-field region, the sign of conventional and remanent hysteresis loops is reversed. In contrast, when the applied H-field is smaller than the coercive field (H_c) of the LSMO film, the sign of two loops is identical. Thus, by appropriate selection of applied field, two stable M_R alignment states in a single LSMO film are selected: antiparallel M_R to the H-field and parallel M_R to the H-field.

As the final step, we investigated the relationship between the crystallinity of this intermediate layer and this unexpected magnetic configuration. The lattice parameter as a function of temperature and thickness was measured by x-ray diffraction (XRD) with E=9 keV at beamline X21 at NSLS. Figure 4(a) and 4(b) show the (001) and (111) Bragg peaks of STO and LSMO. By examining both the (111) and (001) data sets, we can monitor the behavior of the in-plane and out-of-plane lattice parame-

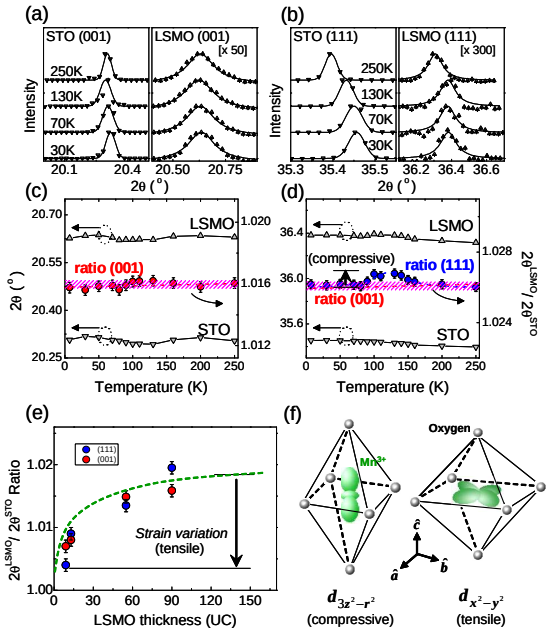

FIG. 4: (Color online) The (001), (a), and (111), (b), Bragg peaks of STO and LSMO as a function of T. Solid lines are fitting results, using a combination of gaussian and lorentzian resolution function. (c) 2θ-positions (left-axis) of STO(001) and LSMO(001). Pink colored shadow denotes the ratio (right-axis) of $2\theta^{\mathrm{LSMO}}/2\theta^{\mathrm{STO}}$. (d) 2θ-positions of (111) peaks and the ratio between them. (e) Strain behavior of differing LSMO thickness. Dashed line is guide to the eye. (f) Relationship between orbital character and strain.

ters for the film and substrate. To highlight the influence of the substrate, we plot in Fig. 4(c) and 4(d) the 2θ values for the film and substrate, as well as their ratio. The ratio should have a linear relationship if the lattice of the film is locked to the substrate, as we show in the (001) data set for this film. A deviation from linearity indicates a separation in the thermal response of the film and substrate. We observe such an anomaly in the (111) data set at 125K. Interestingly, this is the same temperature as the onset of the reversal in the remanent magnetic state (T_{a}). The XRD data indicate that in this temperature range, the LSMO undergoes a compressive fluctuation of the in-plane lattice. However, this anomaly is *not* due to a strain effect from the substrate. In Fig. 4(e) we plot the ratios of the 2θ values for the film and substrate for differing film thickness at room temperature. The films do indeed show a strain behavior, but the strain decreases monotonically with increasing thickness and is relaxed by 90 UC. Hence, we believe that the structural fluctuation for the in-plane LSMO lattice at 125K, and not the substrate-induced strain, may be responsible for the reversed magnetic configuration at remanence.

While the origin of the unusual magnetic configuration at remanence is not entirely clear, we can comment on the role of the structural anomaly and the variation of Mn valence. As the Mn^{3+} distribution in the epitaxial LSMO layer is not uniform along the surface normal direction, the distribution of the orbital anisotropy in Mn^{3+} state relative to Mn^{4+} likewise is not uniform. Prior reports indicate that the Mn^{3+} valence state has a reconstructed e_g orbital ($d_{3z^2-r^2}$) close to the substrate, leading to a reduction of the unit cell along the a,b plane; *i.e.* an in-plane compression, Fig. 4(f) [26, 27]. Furthermore, the magnetic behavior may be influenced by stronger spin-lattice coupling along the in-plane direction in the Mn^{3+}-rich interfacial region through the larger orbital anisotropy in Mn^{3+} (e_g) relative to Mn^{4+} (t_{2g}) [28, 29]. The near-interface region with the enhanced Mn^{3+} concentration may segregate into inhomogeneous patches where the Mn^{3+}/Mn^{4+} ratio varies laterally, resulting in patches where the magnetic ordering varies from AF (predominantly Mn^{3+} valence) and FM (mixed Mn^{3+}/Mn^{4+}) [30]. If the AF regions near the substrate are considerably larger and dominate the interaction with the mixed valence overlayer, the superexchange coupling between Mn^{3+}-Mn^{3+} sites along the surface normal direction may lead to a net AF alignment between the FM regions in the near-substrate regions and the entire FM distribution of the mixed valence overlayer. Further investigations are underway to investigate the nature of the magnetic configuration of the near interface region to illuminate this unusual magnetic behavior.

In summary, we investigated electronic, magnetic, and structural properties of LSMO using comprehensive, synchrotron-based techniques. Although LSMO is structurally a single-layered film, its electronic distribution is not uniform due to doping instabilities and/or charge transfer at the interface, resulting in the formation of an intermediate layer of around a few UC. The presence of this intermediate layer is crucial to the development of the reversed FM configuration at remanence in the thicker LSMO films. Our findings offer a considerable potential for application to films devices, with potential for new forms of spin coupling and device functionality. Moreover, understanding the origin of this reversal behavior presents a rich opportunity for detailed experimental investigations (*e.g.* magnetic depth profiling, transport studies, *etc.*) and theoretical interpretations.

NSLS, BNL, is supported by the U.S. DOE, Office of Science, Office of BES, under Contract No. DE-AC02-98CH10886. Berkeley was sponsored by the SRC NRI-WIN program as well as by the Director, Office of Science, Office of BES, Materials Sciences Division of the U.S. DOE under Contract No. DE-AC02-05CH11231.

[1] J.-H. Song,T. Susaki, and H. Y. Hwang, Adv. Mater. **20**, 2528 (2008).

[2] I. Bozovic, IEEE Trans. Appl. Supercond. **11**, 2686 (2001).
[3] C. H. Ahn, J.-M. Triscone, and J. Mannhart, Nature **424**, 1015(2003); C. H. Ahn *et al.*, Science **276**, 1100 (1997).
[4] L. M. B. Alldredge *et al.*, Appl. Phys. Lett. **89**, 182504 (2006).
[5] M. Gajek *et al.*, Nat. Mater. **6**, 296 (2007).
[6] M. Coey, Nature **430**, 155 (2004).
[7] J. M. D. Coey *et al.*, Adv. in Phys. **48**, 167 (1999).
[8] Y. Lu *et al.*, Phys. Rev. B **54**, R8357 (1996).
[9] J. M. D. Teresa *et al.*, Phys. Rev. Lett. **82**, 4288 (1999).
[10] A. Tebano *et al.*, Phys. Rev. B **74**, 245116 (2006).
[11] E. Dagotto, T. Hotta, and A. Moreo, Physics Reports, **344**, 1 (2001).
[12] J.-H. Park *et al.*, Nature **392**, 794 (1998).
[13] H. Yamada *et al.*, Science **305**, 646 (2004).
[14] J. J. Kavich *et al.*, Phys. Rev. B **76**, 014410 (2007).
[15] J. X. Ma *et al.*, Phys. Rev. B **79**, 174424 (2009).
[16] P. Yu *et al.*, Phys. Rev. Lett. **105**, 027201 (2010).
[17] S. Langridge *et al.*, Unpublished.
[18] M. Huijben *et al.*, Phys. Rev. B **78**, 094413 (2008).
[19] M. Abbate *et al.*, Phys. Rev. B **46**, 4511 (1992).
[20] C. Aruta *et al.*, Phys. Rev. B **80**, 014431 (2009).
[21] A. Tanaka and T. Jo, J. Phys. Soc. Jpn. **63**, 2788 (1994).
[22] Parameters used in the calculations; $10Dq$, Slater-Koster transfer integral, on-site Coulomb energy, and charge transfer energy are set to 1.0, 3.0, 3.5, and 4.5 eV, respectively, under O_h symmetry.
[23] T. Riedl *et al.*, Microsc. Microanal. **15**, 213 (2009).
[24] L. Samet *et al.*, Eur. Phys. J. B **34**, 179 (2003).
[25] L. G. Parratt, Phys. Rev. **95**, 359 (1954).
[26] C. Aruta *et al.*, Phys. Rev. B **73**, 235121 (2006).
[27] A. Tebano *et al.*, Phys. Rev. Lett. **100**, 137401 (2008).
[28] J. B. Goodenough, Phys. Rev. **100**, 564 (1955).
[29] J.-H. Park *et al.*, Phys. Rev. Lett. **76**, 4215 (1996).
[30] L. Brey, Phys. Rev. B **75**, 104423 (2007).